REVIEW

CrossMark

Structure and dynamics of rotary V$_1$ motor

Hiroshi Ueno[1] · Kano Suzuki[2] · Takeshi Murata[2,3]

Abstract
Rotary ATPases are unique rotary molecular motors that function as energy conversion machines. Among all known rotary ATPases, F$_1$-ATPase is the best characterized rotary molecular motor. There are many high-resolution crystal structures and the rotation dynamics have been investigated in detail by extensive single-molecule studies. In contrast, knowledge on the structure and rotation dynamics of V$_1$-ATPase, another rotary ATPase, has been limited. However, recent high-resolution structural studies and single-molecule studies on V$_1$-ATPase have provided new insights on how the catalytic sites in this molecular motor change its conformation during rotation driven by ATP hydrolysis. In this review, we summarize recent information on the structural features and rotary dynamics of V$_1$-ATPase revealed from structural and single-molecule approaches and discuss the possible chemomechanical coupling scheme of V$_1$-ATPase with a focus on differences between rotary molecular motors.

Keywords Rotary catalysis · Ion pump · *Enterococcus hirae* · Crystal structure · Single-molecule technique

Abbreviations
AMPPNP Adenosine 5′-(β,γ-imido)triphosphate
ATPγS Adenosine 5′-*O*-(3-thio)triphosphate

Introduction

All living cells use a chemical fuel called adenosine triphosphate (ATP) to maintain the functions required for life, such as protein biosynthesis, muscle contraction, and brain activity. Therefore, ATP is often referred to as the energy currency for the cell. Under aerobic conditions, the majority of ATP is produced by the F-type ATP synthase [1]. F-type ATP synthases (also known as F-ATPases) are ubiquitous rotary motor enzymes found in the inner membrane of mitochondria, the thylakoid membrane of chloroplasts, and the plasma membranes of bacteria. They catalyze ATP synthesis from ADP and inorganic phosphate using the energy of ion (proton or sodium) translocation caused by transmembrane

electrochemical potential (proton or sodium ions) and, when operating in reverse, they also generate an electrochemical potential difference of ions using the energy released by ATP hydrolysis [2–4].

Eukaryotic vacuolar-type ATPases (V-ATPases) are also rotary motor enzymes; they are evolutionarily and functionally related to F-type ATP synthases [5, 6]. They function in reverse of F-type ATP synthases, that is, they transport ions (protons or sodium ions) across the membrane using the energy derived from ATP hydrolysis. Acidification of vesicles by intracellular V-ATPases is important for various cellular processes, including receptor-mediated endocytosis, membrane trafficking, and protein processing and degradation. They also function on the plasma membrane of certain cells, such as tumor cells, renal intercalated cells, and osteoclasts. Aberrant function of V-ATPase is associated with a number of human diseases including tumor metastasis, distal renal tubular acidosis, and osteoporosis. Therefore, they are considered as potential drug targets [5, 7]. V-ATPases are found in some bacteria, such as *Thermus thermophilus* (*T. thermophilus*) and *Enterococcus hirae* (*E. hirae*). V-ATPase from *T. thermophilus* functions as an ATP synthase under physiological conditions [8, 9]. Therefore, this enzyme is sometimes called A-type ATPase found in Archeae (A-ATPase). A-ATPases function as ATP synthases similar to the F-type ATP synthase, although the structure and subunit composition of A-ATPases are more similar to

✉ Hiroshi Ueno
hueno@nojilab.t.u-tokyo.ac.jp

1 Department of Applied Chemistry, Graduate School of Engineering, University of Tokyo, Tokyo 113-8656, Japan

2 Department of Chemistry, Graduate School of Science, Chiba University, Chiba 263-8522, Japan

3 JST, PRESTO, Chiba 263-8522, Japan

those of V-ATPases (Fig. 1a) [10–12]. V-ATPase from *E. hirae* functions as a sodium ion pump similar in nature to eukaryotic V-ATPase, and plays an important role in maintaining sodium homeostasis in cells under an alkaline environment [13–15].

All rotary ATPases are unique rotary molecular motors that function as energy conversion machines with a similar architecture and rotary catalytic mechanism [5, 11, 12, 16]. They are large, multi-subunit complexes composed of a hydrophilic $F_1/V_1/A_1$ motor for ATP synthesis/hydrolysis and a membrane-embedded $F_o/V_o/A_o$ motor for ion transport. The bacterial $F_1/V_1/A_1$ and $F_o/V_o/A_o$ motors are connected by one central stalk and one or two peripheral stalks (Fig. 1). Interestingly, V-ATPases in eukaryotes have three peripheral stalks, although there is only one peripheral stalk in eukaryotic F-ATPases [16–18]. The peripheral stalks of eukaryotic V-ATPases play an important role in reversible dissociation of V_1 motor from V_o motor with silencing of the ATP hydrolysis activity of the free V_1 motor [18], in contrast to F_1 motor which will rapidly hydrolyze ATP when isolated. This implies the fact that it was necessary for V-ATPases to evolve a regulatory mechanism for keeping the dissociated V_1 motors catalytically inactive to prevent wasteful energy consumption.

Among all known rotary ATPases, the hydrophilic portion of F-ATPase (F_1-motor or F_1-ATPase) is the best characterized; there are high-resolution crystal structures of several rotational states [19–28] and the chemomechanical coupling scheme has been revealed in detail by extensive single-molecule studies [29–40]. Relatively little is known about the structure and rotation scheme of V_1-motors (V_1-ATPase) [41–43]. Recently, high-resolution crystal structures of

several rotational states of V_1-ATPase from *E. hirae* have been determined [44, 45]. Furthermore, basic rotary dynamics of this V_1-ATPase have been revealed by single-molecule studies [46–49]. These studies have provided new insights into the rotation mechanism of V_1-ATPase. In the present review, we discuss recent findings on the structural features and rotary dynamics of bacterial V_1-ATPase revealed from structural and single-molecule studies with a focus on differences from the properties of F_1-ATPase.

V_1-ATPase: structural studies

In the bacterial V-ATPase, the catalytic V_1 moiety is composed of A, B, D, and F subunits, in which three alternately arranged A and B subunits form a hexameric stator A_3B_3 ring. The central rotary shaft of D and F subunits penetrates the central cavity of the A_3B_3 ring and rotates using the energy of ATP hydrolysis [41–44]. Unlike the isolated eukaryotic V_1 moiety in which subunit H inhibits its activity [18], the isolated bacterial V_1 moiety can generally catalyze ATP hydrolysis and hence is called V_1-ATPase. Structural studies have been conducted using a V_1-ATPase from the thermophilic eubacterium *T. thermophilus*, which has high stability. The crystal structure of the A_3B_3 subcomplex from *T. thermophilus* was determined at 2.8 Å resolution [41]. The diameter of the A_3B_3 subcomplex is larger than that of the $\alpha_3\beta_3$ subcomplex in F_1-ATPase, because it includes an outward protrusion domain in the A subunit (Fig. 2a, green circles), termed the "non-homologous region" that is absent from β subunit; the structure also provides molecular information
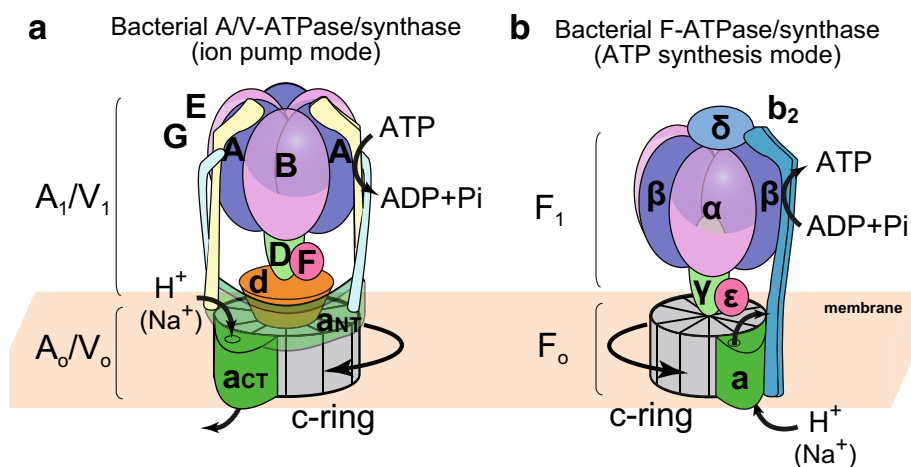
Fig. 1 Schematic illustrations of bacterial rotary ATPases. **a** A/V-type ATPases/synthases are found in Archeae and some bacterial taxa. They are composed of a soluble catalytic core A_1/V_1 motor (A_3B_3DF) and a membrane integral A_o/V_o motor (ac_nd; where *n* is the copy number of the c subunits). The A_1/V_1 and A_o/V_o motors are connected by the two peripheral stalks (EG). The N- and C-terminal domains of a subunit are shown as a_{NT} and a_{CT}, respectively. **b** Bacterial F-type ATPases/synthases are structurally different from bacterial A/V-type ATPases/synthases. The F_1 ($\alpha_3\beta_3\gamma\delta\epsilon$) and F_o motors (ab_2c_n) are connected by only one peripheral stalk (b_2)
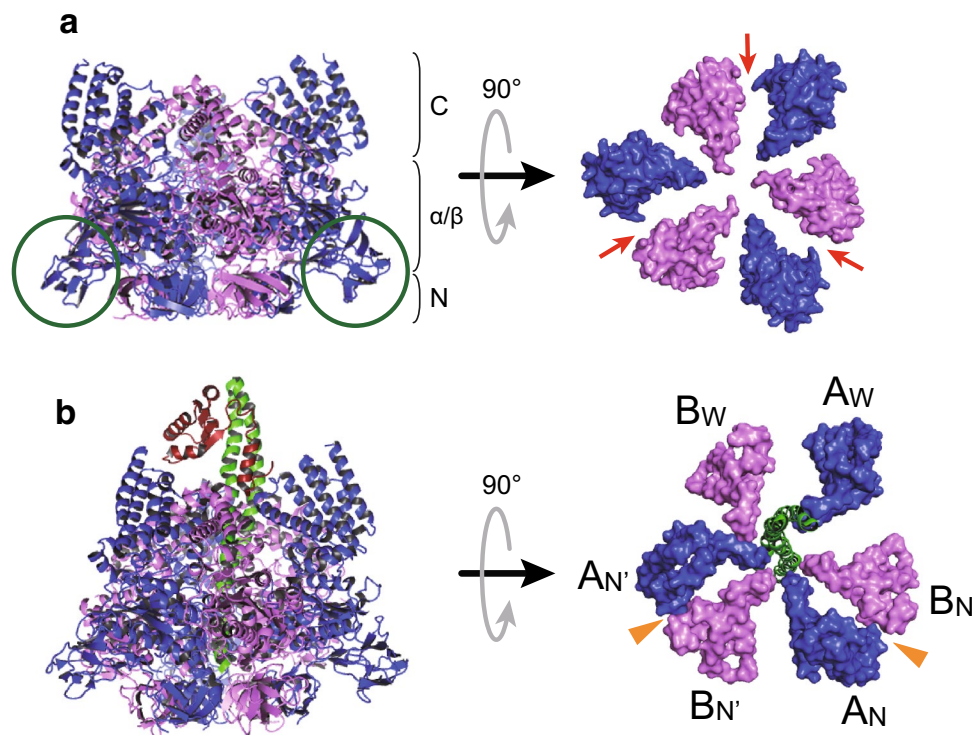
Fig. 2 Crystal structures of A₃B₃ subcomplex and V₁-ATPase from *T. thermophilus*. **a** Crystal structure of the nucleotide-free A₃B₃ subcomplex from *T. thermophilus* determined at 2.8 Å resolution (PDB ID: 3GQB) [41]. Side view (left) and Top view (right) from the membrane side. Only the C-terminal domains of the A₃B₃ ring are shown in top view to clarify the distinct conformations of individual A or B subunits. The A and B subunits are shown in blue and magenta, respectively. Each A and B subunit consists of the N-terminal β-barrel (N), the central α/β domain (α/β), and the C-terminal helical domain (C). Green circles indicate the "non-homologous region" in the A subunit. Red arrows indicate the catalytic sites. **b** Overall structure of V₁-ATPase (A₃B₃DF) from *T. thermophilus* determined at 4.5 Å resolution (PDB ID: 3A5C) [42]. Side view (left) and top view (right) from the membrane side. Only the C-terminal domains of the A₃B₃ ring and the D subunit are shown in top view. The A, B, D, and F subunits are shown in blue, magenta, green, and red, respectively. A$_W$, B$_W$ pair shows a wide-open conformation, as observed in a α$_E$β$_E$ pair in F₁-ATPase [19]. A$_N$B$_N$ and A$_{N'}$B$_{N'}$ pairs show a narrowly closed conformation, as do the α$_{TP}$β$_{TP}$ and α$_{DP}$β$_{DP}$ pairs in F₁-ATPase [19]. The crystals were obtained by co-crystallization with Mg²⁺ ADP and aluminium fluoride. Strong electron densities which presumably correspond to the phosphate groups of bound-ADP were found in the A$_N$B$_N$ and A$_{N'}$B$_{N'}$ pairs (orange arrowheads)

about the B–A interface. The catalytic sites are located at the interfaces of the A and B subunits (Fig. 2a, red arrows), with the majority of the catalytic residues residing in the A subunits, similar to the catalytic β subunits and the non-catalytic α subunits in F₁-ATPase [19, 27]. The overall structure of V₁-ATPase (A₃B₃DF complex) from *T. thermophilus* was first determined at 4.5–4.8 Å resolution (Fig. 2b) [42]. This structure provided the initial information about the position and orientation of the rotor DF subunits in the A₃B₃ ring and revealed structural similarities and differences between V₁- and F₁-ATPase. However, the lack of high-resolution structural information for the overall V₁-ATPase from *T. thermophilus* limits our understanding of its molecular architecture and operation. Meanwhile, high-resolution crystal structures of the A₃B₃ ring and entire V₁-ATPase from *E. hirae* have recently been solved with and without bound nucleotides [44, 45].

Structure of A₃B₃ ring from *E. hirae*: asymmetric structure

The high-resolution crystal structures of the A₃B₃ ring from *E. hirae* were solved with and without a non-hydrolyzable ATP analog [adenosine 5′-(β,γ-imido)triphosphate or AMPPNP] at 3.4 and 2.8 Å resolution, respectively (Fig. 3) [44]. The overall architecture of A₃B₃ from *E. hirae* is similar to that of α₃β₃ in F₁-ATPase, but the structures show some differences.

Each A and B subunit consists of an N-terminal β-barrel, central α/β domain, and C-terminal helical domain (Fig. 3a, right). Superimposition of the N-terminal β-barrel part of three A or B subunits shows that the conformations of each A and B subunit are not identical. If one of the A subunits is in the closed conformation (C),
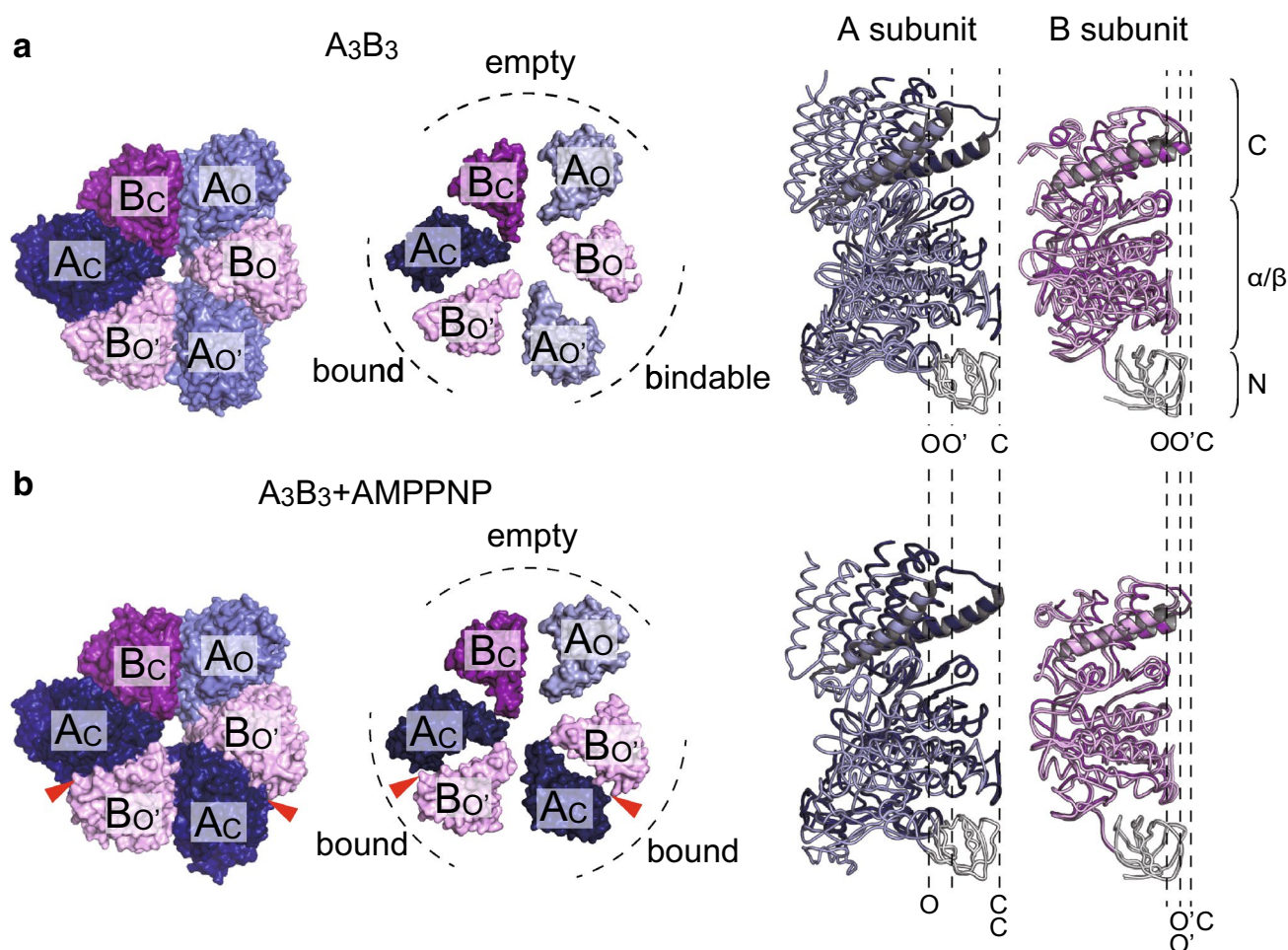
Fig. 3 Crystal structures of A_3B_3 subcomplex from *E. hirae*. **a** Crystal structure of the nucleotide-free A_3B_3 subcomplex from *E. hirae* determined at 2.8 Å resolution (PDB ID: 3VR2) [44]. Each A and B subunit consists of the N-terminal β-barrel (N), the central α/β domain (α/β), and the C-terminal helical domain (C) as seen in A_3B_3 from *T. thermophilus* (Fig. 2a). **b** Crystal structure of the nucleotide-bound A_3B_3 subcomplex from *E. hirae* determined at 3.4 Å resolution (PDB ID: 3VR3) [44]. Two AMPPNP molecules are bound to the 'bound' sites (indicated by red arrowheads). Top views from the membrane side are shown on the left and center. Only the C-terminal domains of the A_3B_3 rings are shown in the center to clarify the distinct conformations of individual A or B subunits and the different structures of the three catalytic sites. On the right, conformations of the individual A and B subunits superimposed at the N-terminal β-barrel domain (white) are shown. *O and O′* open conformation, *C* closed conformation

the other two A subunits show open conformations (O or O′). Similarly, one of the B subunits takes the closed form (C) and the other two take open conformations (O or O′) (Fig. 3a), resulting in the asymmetry of the A_3B_3 ring. Interestingly, even in the absence of nucleotides and central rotor DF subunits, each catalytic site shows the three distinct states. In contrast, F_1-ATPase shows a threefold symmetric structure with three identical catalytic sites in the absence of bound nucleotides [50, 51]; accordingly, the asymmetric structure of the stator ring is not observed in the case of F_1-ATPase. In the presence of high concentration of AMPPNP (5 mM), the A_3B_3 ring binds two AMPPNP molecules (Fig. 3b), resulting in changes in the conformation of A (O′ to C) and B (O to O′) subunits, but

the $A_CB_{O'}$ pair shows little conformational change upon AMPPNP binding. Therefore, the three catalytic sites (A_OB_C, $A_{O'}B_O$, and $A_CB_{O'}$) are termed 'empty', 'bindable', and 'bound' sites, respectively (Fig. 3a, b).

Two AMPPNP-bound structure of V_1-ATPase: catalytic dwell state

In addition to the A_3B_3 ring structures, the nucleotide-free entire V_1-ATPase from *E. hirae* (eV_1) was also determined at 2.2 Å resolution [44]. Insertion of the rotor DF subunits into the stator A_3B_3 ring induces conformational changes in the A and B subunits, even in the absence of bound nucleotides
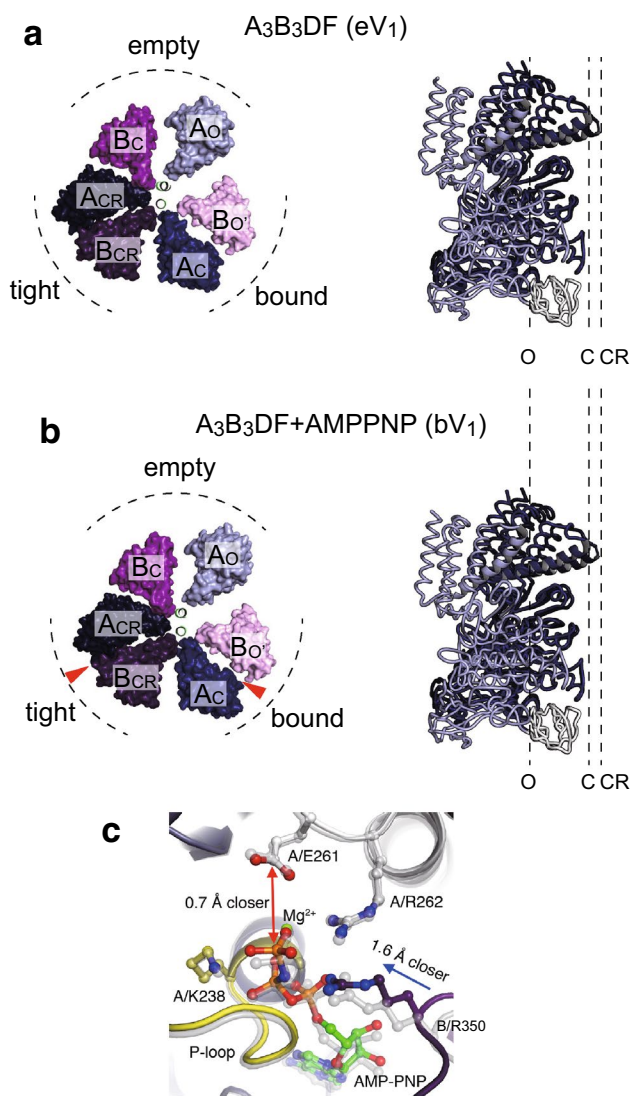
Fig. 4 Crystal structures of entire V$_1$-ATPase from *E. hirae*. **a** Crystal structure of the nucleotide-free V$_1$-ATPase from *E. hirae* determined at 2.2 Å resolution (PDB ID: 3VR4) [44]. **b** Crystal structure of the nucleotide-bound V$_1$-ATPase from *E. hirae* determined at 2.7 Å resolution (bV$_1$, PDB ID: 3VR6) [44]. Two AMPPNP molecules are bound to the 'bound' and the 'tight' sites (indicated by red arrowheads). Top views from the membrane side are shown on the left. Only the C-terminal domains of the A$_3$B$_3$ rings and the α-helical coiled-coil portion of the D subunit are shown. On the right, conformations of the individual A subunit superimposed at the N-terminal β-barrel domain (white) are shown. *O* open conformation, *C* closed conformation, *CR* more closed 'closer' conformation. Two AMPPNP-bound V$_1$-ATPase shows an almost identical structure to the nucleotide-free V$_1$-ATPase. **c** Nucleotide-binding site of the bV$_1$ (PDB ID: 3VR6). Superposition of the 'bound' site (transparent grey) and the 'tight' site (colored) of the bV$_1$

(Fig. 4a). This results in changes in the conformations of A and B subunits from the closed (C) to the more closed 'closer' (CR) conformation and from the open (O') to closer (CR) conformation, respectively. Consequently, eV$_1$ shows three different catalytic sites termed 'empty', 'bound', and 'tight' sites (Fig. 4a). Furthermore, by soaking eV$_1$ in AMPPNP, the structure of nucleotide-bound V$_1$-ATPase (bV$_1$ or 2$_{ATP}$V$_1$) was also determined at 2.7 Å resolution (Fig. 4b) [44, 45]. Two AMPPNP molecules were bound to the binding sites of the 'bound' and 'tight' sites of eV$_1$, but the overall structure was very similar to that of eV$_1$ (Fig. 4a, b). Even in the presence of high AMPPNP (2 mM), no electron density peak for AMPPNP was found in the 'empty' site, indicating that it has a very low affinity for AMPPNP. Comparison of the 'tight' and 'bound' sites in bV$_1$ revealed the movement of the Arg-finger (Arg-350) in the 'tight' site closer to the γ-phosphate relative to the 'bound' site (Fig. 4c). This γ-phosphate moved closer to Glu-261 in the A subunit which is essential for ATPase activity in yeast V$_1$-ATPase [52]. The corresponding Glu-188 of the β subunit in bovine mitochondrial F$_1$-ATPase is an essential residue for ATP hydrolysis and interacts with the γ-phosphate of the nucleotide and lytic water molecules [19, 28, 53]. The closer proximity of the Arg-finger to the γ-phosphate may enhance the ATP hydrolysis reaction. Therefore, it is possible that the 'tight' site corresponds to the catalytic site waiting for ATP hydrolysis and this structure corresponds to the catalytic dwell state (Fig. 5a). Similar nucleotide-free and nucleotide-bound structures of yeast mitochondrial F$_1$-ATPase have been reported [25]. These results suggest that interactions between the rotor and stator are as crucial as nucleotide binding for determining the structure of the catalytic sites of rotary ATPases.

Two ADP-bound structure of V$_1$-ATPase: ATP-binding dwell state

More recently, the crystal structures of two other nucleotide-bound states were reported [45], i.e., the two ADP-bound structure (2$_{ADP}$V$_1$) and the three ADP-bound structure (3$_{ADP}$V$_1$). When soaking the eV$_1$ crystals in 20 μM ADP, it binds to the 'bound' and 'tight' sites of eV$_1$, as in the case of bV$_1$, and the two ADP-bound structure was solved at 3.3 Å resolution (Fig. 5b). ADP binding to the 'tight' site in eV$_1$ induces changes in the A and B subunits to more open conformations (CR to C in A subunit; CR to C′ in B subunit), but the 'bound' site in eV$_1$ shows no conformational change upon ADP binding. The observed conformational changes result in the tilting of rotor DF subunits towards the ADP-bound site (A$_C$B$_{C′}$) (Fig. 5b). Interestingly, the 'empty' site shows a cooperative conformational change without ADP binding. The newly found catalytic sites (A$_C$B$_{C′}$ and A$_{O′}$B$_{O″}$) are termed 'ADP-bound' and 'bindable-like' sites, respectively. The 'bindable-like' site is similar to the 'bindable' site in the A$_3$B$_3$ structure (Fig. 3a) and takes a more open conformation
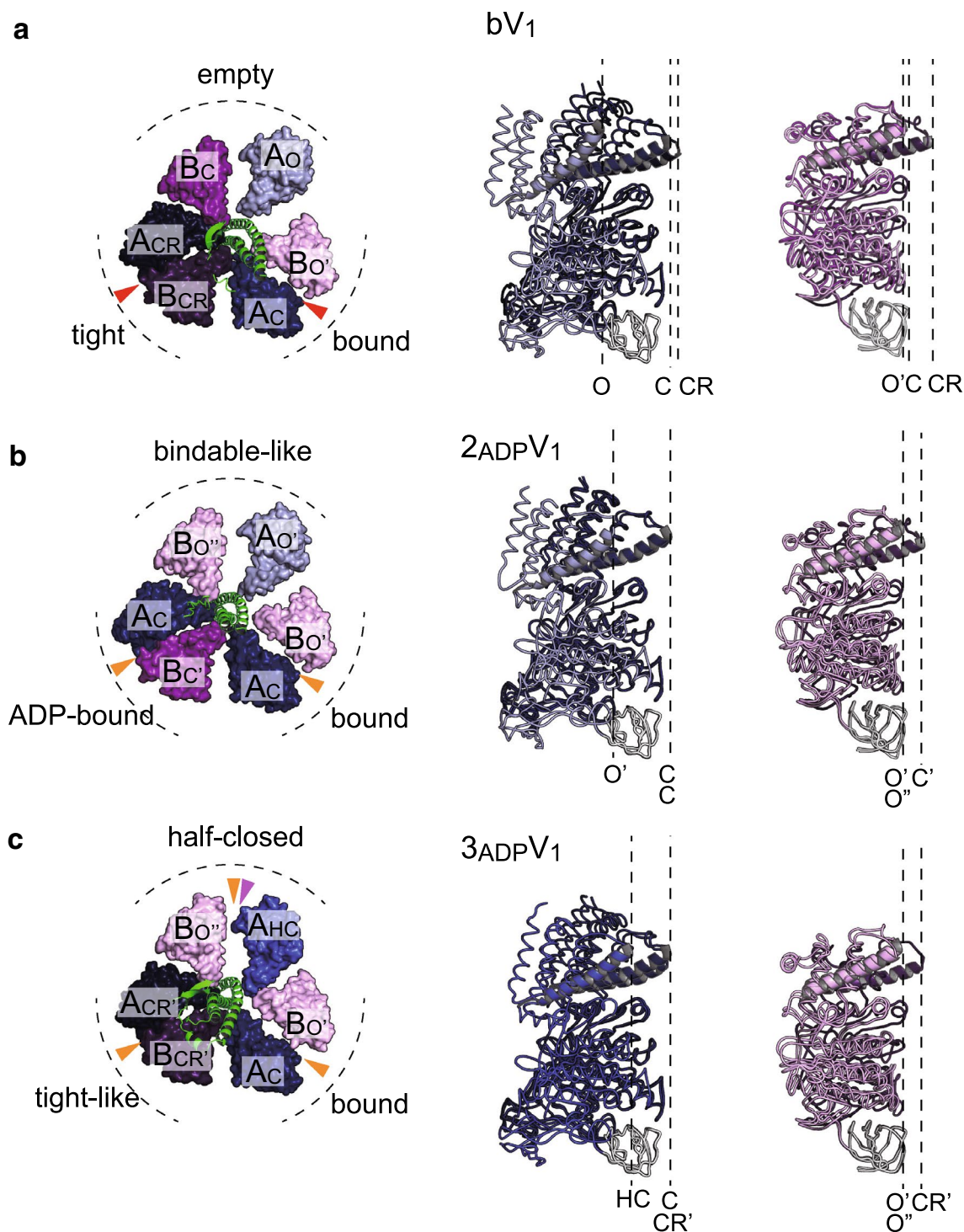
Fig. 5 Crystal structures of two AMPPNP-bound V_1-ATPase (bV_1), two ADP-bound V_1-ATPase ($2_{ADP}V_1$), and three ADP-bound V_1-ATPase ($3_{ADP}V_1$) from *E. hirae*. **a** Crystal structure of two AMPPNP-bound V_1-ATPase (bV_1, 2.7 Å resolution, PDB ID: 3VR6) [44]. **b** Crystal structure of two ADP-bound V_1-ATPase ($2_{ADP}V_1$, 3.3 Å resolution, PDB ID: 5KNB) [45]. **c** Crystal structure of three ADP-bound V_1-ATPase ($3_{ADP}V_1$, 3.0 Å resolution, PDB ID: 5KNC) [45]. Top views of the C-terminal domain of A_3B_3 rings and central rotor D subunit (green) viewed from the membrane side are shown on the left. Red, orange, and magenta arrowheads indicate the catalytic sites that bind to AMPPNP, ADP, and sulfate, respectively. Conformations of the individual A and B subunits superimposed at the N-terminal β-barrel domain (white) are shown on the right. *O and O′* open conformation, *HC* half-closed conformation, *C* closed conformation, *CR* more closed 'closer' conformation

Three ADP-bound structure of V$_1$-ATPase: ADP-release dwell state

The $3_{ADP}V_1$ structure was solved at 3.0 Å resolution by soaking the eV$_1$ crystals in 2 mM ADP [45]. In this structure, all three catalytic sites are occupied by ADP and, in addition, a sulfate is bound to one catalytic site (Fig. 5c, magenta arrowhead). A comparison between $2_{ADP}V_1$ and $3_{ADP}V_1$ structures shows that ADP (and sulfate) binding to the 'bindable-like' site in $2_{ADP}V_1$ induces a conformational change in the A subunit (O′) to the 'half-closed' conformation (HC), whereas the B subunit (O″) shows no conformational change. This catalytic site ($A_{HC}B_{O″}$) in $3_{ADP}V_1$ is termed a 'half-closed' site. The conformational change in the catalytic site from the 'bindable-like' site to the 'half-closed' site induces a conformational change of the 'ADP-bound' site to a more tight-like conformation ($A_{CR′}B_{CR′}$). This shifted 'ADP-bound' site in $3_{ADP}V_1$ is termed a 'tight-like' site, because the nucleotide-binding site is more similar to that of the 'tight' site than to that of the 'ADP-bound' site (Fig. 6). The β-phosphate of ADP in the 'tight-like' site is more distant from the surrounding interacting residues compared to that in the 'ADP-bound' site, suggesting that an ADP will be easily released from the 'tight-like' site (Fig. 6) [45]. Therefore, the "tight-like" site is considered to be a dwelling state before ADP release and the $3_{ADP}V_1$ structure is regarded as the ADP-release dwell state.

Structural difference between F$_1$-and V$_1$-ATPase: conformational features

A comparison of the two AMPPNP-bound structures of V$_1$-ATPase from *E. hirae* [44, 45] and F$_1$-ATPase from bovine mitochondria [28] is shown in Fig. 7. Both nucleotide-binding sites show very similar arrangements of catalytically important residues and nucleotides (Fig. 7a). However, the overall structures of A and B subunits in V$_1$-ATPase show some differences from those of the β and α subunits in F$_1$-ATPase. The non-catalytic B subunit of this V$_1$-ATPase does not bind to a nucleotide, whereas the non-catalytic α subunit of F$_1$-ATPase binds to a nucleotide (Fig. 7b). Superimposition of the N-terminal β-barrel part of three A and B subunits in V$_1$-ATPase and β and α subunits in F$_1$-ATPase reveals conformational differences between A_C and A_{CR}, and B_C and B_{CR} of V$_1$-ATPase, but the conformations of $β_{TP}$ and $β_{DP}$ as well as $α_{TP}$ and $α_{DP}$ of F$_1$-ATPase are very similar (Fig. 7c). These differences are also evidenced by the positional displacement of residues between two of the three A and B subunits in V$_1$-ATPase and β and α subunits in F$_1$-ATPase (Fig. 8), which also shows that the structures of A_C and A_{CR} are largely different from that of A_O (Fig. 8, top left). In contrast, the central portions (residues 180–320) of the $β_{TP}$ and $β_{DP}$ structures show very similar conformations to that of the $β_E$ structure (Fig. 8, top right). These results suggest that the A subunit in V$_1$-ATPase from *E. hirae* undergoes the whole conformational change upon nucleotide binding, whereas the β subunit in F$_1$-ATPase undergoes the conformational change mainly in the P-loop and C-terminal domains.

Thus, the conformational features of the A and B subunits in V$_1$-ATPase from *E. hirae* are apparently different from those of the β and α subunits in bovine F$_1$-ATPase, despite the highly similar nucleotide-binding sites of these ATPases. These structural differences and similarities may be related

Fig. 6 Nucleotide-binding site of the three ADP-bound V$_1$-ATPase ($3_{ADP}V_1$). Nucleotide-binding site of the "tight-like" site in $3_{ADP}V_1$ (colored) is superimposed at the adenosine onto those (transparent grey) of the "ADP-bound" site in $2_{ADP}V_1$ (left) and the "tight" site in bV$_1$ (right)
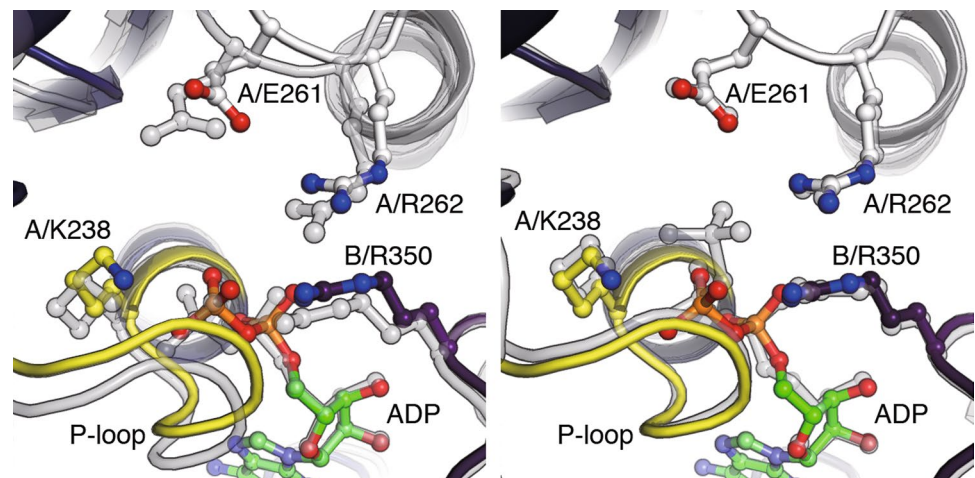
Fig. 7 Structural differences between F$_1$- and V$_1$-ATPase. **a** Comparison of the nucleotide-binding site of the "tight" site in *E. hirae* V$_1$-ATPase (bV$_1$, PDB ID: 3VR6) with that of the "ADP-bound" site in bovine F$_1$-ATPase (PDB ID: 2JDI) [28]. **b** Top views from the membrane side of bV$_1$ (left) and bovine F$_1$-ATPase (right). The catalytic and non-catalytic sites that bind to AMPPNP molecules are indicated by red arrowheads. **c** Superimposed structures at the N-terminal β-barrel (white) of three structures of A and B subunits in bV$_1$ compared with the β and α subunits in F$_1$-ATPase
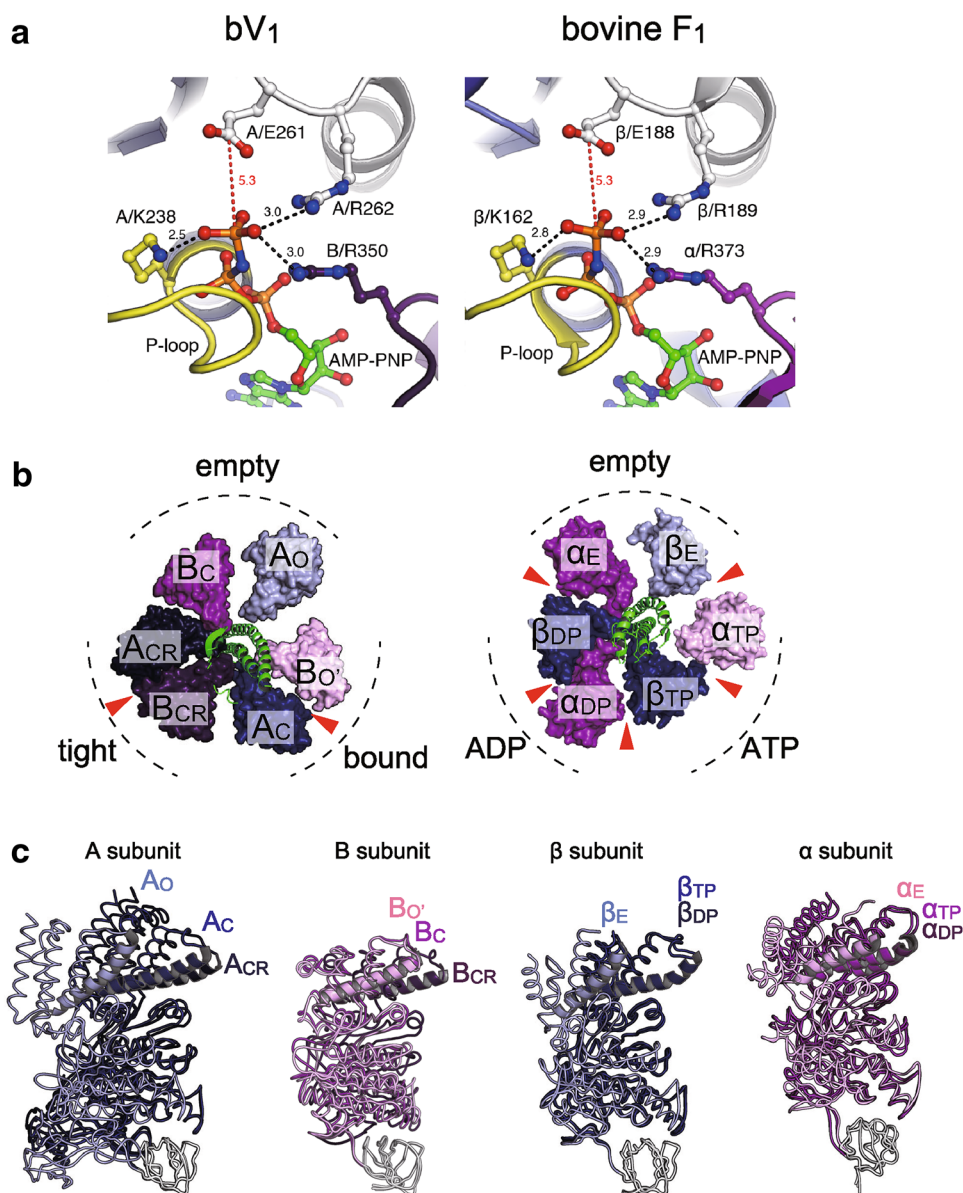
to the 'unique' and 'common' mechanisms of rotary catalysis between these rotary ATPases, such as the chemomechanical coupling scheme of the rotation [40, 46].

Dynamics of rotary V$_1$-ATPase: single-molecule studies

After the establishment of the single-molecule rotation assay of F$_1$-ATPase in 1997 [29], the dynamics of rotary ATPases from various species have been studied at the single-molecule level [38–40, 46, 54–57]. The first rotation of V$_1$-ATPase has been directly visualized under an optical microscope by the attachment of large beads to the rotor DF subunits in V$_1$-ATPase from *T. thermophilus*

[58]. V$_1$-ATPase from *T. thermophilus* rotates stepwise in a counterclockwise direction, consuming one ATP molecule at each step when viewed from the membrane side. The basic step size is 120°, which is similar to that of F$_1$-ATPase, and no substeps have been resolved in the rotation, even when using a slowly hydrolyzable ATP analog (adenosine 5′-*O*-(3-thio)triphosphate or ATPγS) and high-speed imaging of gold nanoparticles [48, 59]. These results indicate that ATP binding and ATP cleavage (and/or phosphate release) occur at the same angle in this V$_1$-ATPase. In the case of F$_1$-ATPases, some or all of these elementary reaction steps occur at different angles and the basic 120° step is further divided into two or three substeps [31, 32, 39, 40], i.e., 80° and 40° substeps in thermophilic *Bacillus* PS3 F$_1$-ATPase [31, 32], 85° and 35° substeps in *Escherichia coli* F$_1$-ATPase [39], and
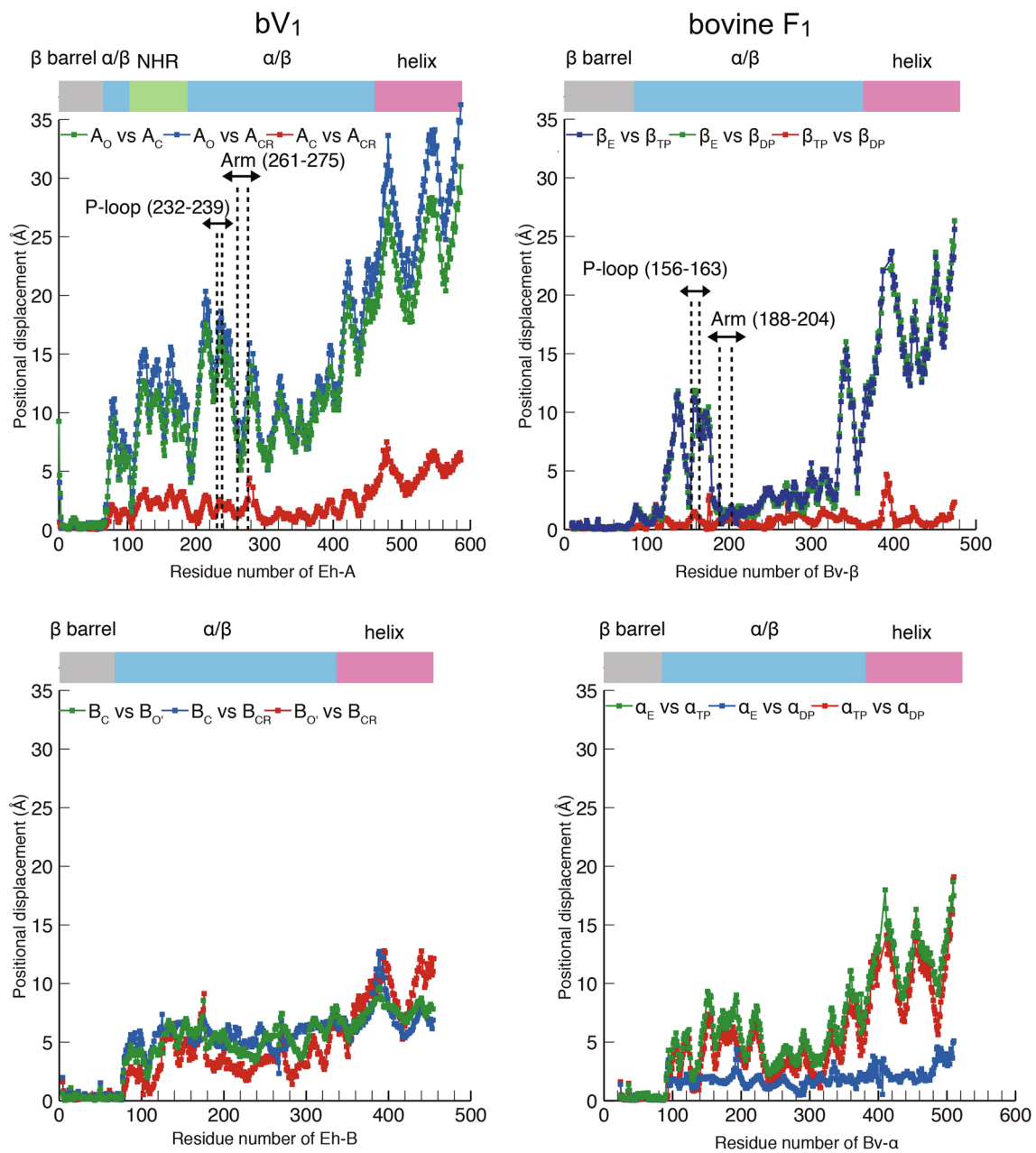
Fig. 8 Comparison of the conformational differences between F₁- and V₁-ATPase. Positional displacement of residues (Cα atoms) between two of the three A subunits (top left) and B subunits (bottom left) in bV₁, and β subunits (top right) and α subunits (bottom right) in bovine F₁-ATPase (PDB ID: 2JDI), which are superimposed at the N-terminal β-barrel domains (see Fig. 7c)

65°, 25°, and 30° substeps in human F₁-ATPase [40]. The 80°, 85°, and 65° substeps are triggered by ATP binding and ADP release, while the 40° and 35° substeps are triggered by ATP cleavage and phosphate release. In human F₁-ATPase, it is proposed that ATP cleavage and phosphate release trigger different substeps of 30° and 25°, respectively.

Recently, rotary dynamics of V₁-ATPase from *E. hirae* have been characterized using single-molecule analyses at a submillisecond temporal resolution employing gold nanoparticles and an objective-type total internal reflection dark field microscope (Fig. 9a) [46–48]. V₁-ATPase from *E. hirae* rotates in basically the same manner as that from *T. thermophilus* which functions as ATP synthase [55, 59]. This V₁-ATPase also shows only three pauses separated by 120° at all concentrations ranging from below to above the Michaelis constant (K_m), where distinct elementary reaction steps of ATP hydrolysis (ATP binding, ATP cleavage, or product release) become the rate-limiting step (Fig. 9b),

Fig. 9 Single-molecule rotation of *E. hirae* V_1-ATPase. **a** Schematic illustration of the single-molecule rotation assay of *E. hirae* V_1-ATPase. The A_3B_3 ring is immobilized on a glass surface via a His-tag on the A subunit, and an optical probe (gold nanoparticle, 40 nm in diameter) is attached to the D subunit to visualize the rotary motion of rotor DF subunits using an optical microscope [46, 68]. **b** Rotations of *E. hirae* V_1-ATPase for various concentrations of ATP. Left: 40 mM ATP, considerably higher than the Michaelis constant (K_m, 154 μM). Center: 100 μM ATP, near the K_m. Right: 10 mM ATP, considerably lower than the K_m [46]
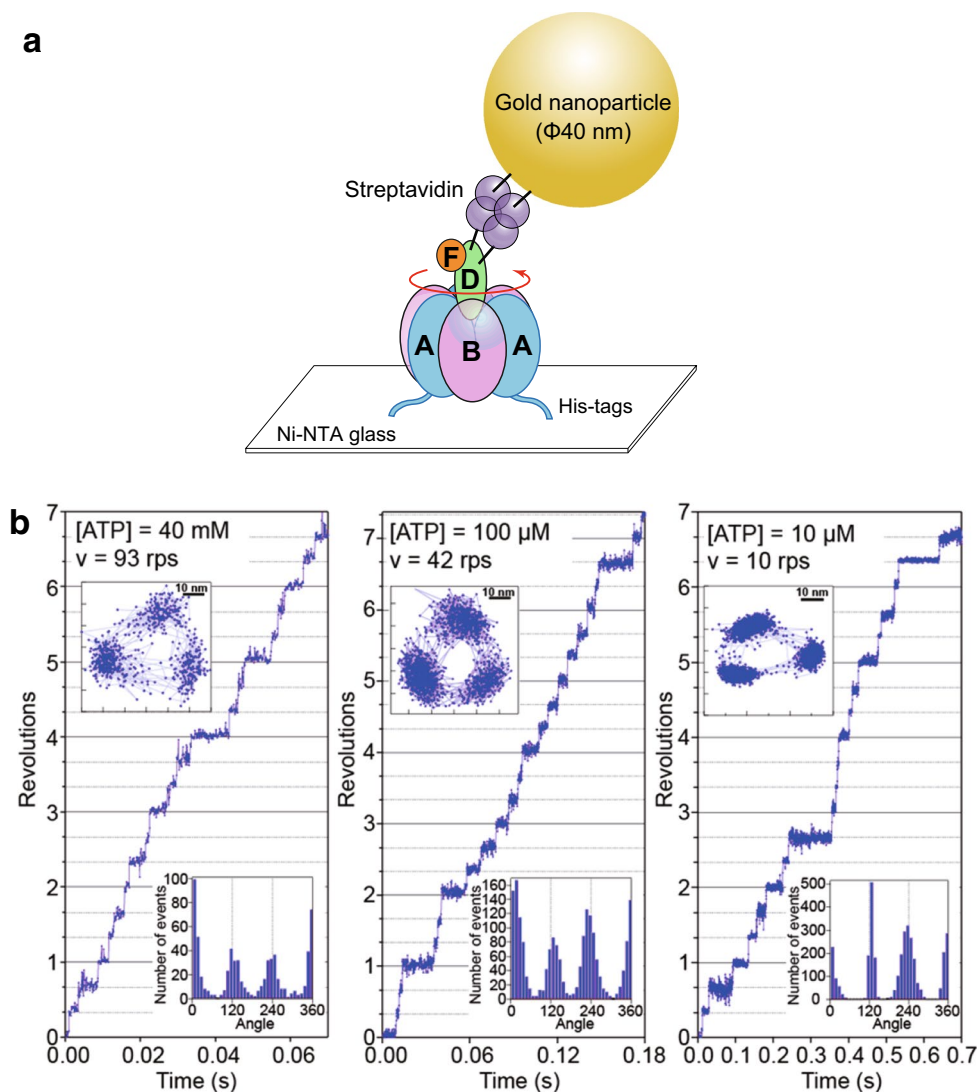
suggesting that 120° stepping rotation without substeps is a common property of V_1-ATPase [46], despite the difference in physiological function between V-ATPase from *E. hirae* (ion pump) and that from *T. thermophilus* (ATP synthesis). These results imply that the basic properties of rotary dynamics of F-ATPases and V-ATPases are determined by their overall structures and that the difference in physiological function derives from regulatory mechanisms such as Mg^{2+} ADP inhibition and inhibitor proteins [9, 18, 23, 26].

Chemomechanical coupling scheme of V_1-ATPase

Figure 10a shows a proposed chemomechanical coupling scheme of V_1-ATPase from *E. hirae* based on recently determined structural features and rotary dynamics [44–47]. As mentioned above, three distinct structures of *E. hirae*

V_1-ATPase have been solved ($bV_1 = 2_{ATP}V_1$, $2_{ADP}V_1$, and $3_{ADP}V_1$) [44, 45]. These three structures are regarded as the three different dwelling states in the rotation waiting for the elementary reaction steps of ATP hydrolysis corresponding, respectively, to the catalytic (ATP cleavage) dwell ($bV_1 = 2_{ATP}V_1$), ATP-binding dwell ($2_{ADP}V_1$), and ADP-release dwell ($3_{ADP}V_1$) states.

In this model, ATP binds to the 'bindable-like' site in $2_{ADP}V_1$, which induces conformational changes of 'bindable-like' and 'ADP-bound' sites to 'half-closed' and 'tight-like' sites, respectively. This results in a slight shift of the rotor DF subunits toward the 'tight-like' site, but does not induce the obvious rotation of the rotor DF subunits. Then, ADP release occurs at the 'tight-like' site in $3_{ADP}V_1$, and all three catalytic sites change the conformations from 'half-closed' to 'bound', from 'bound' to 'tight', and from 'tight-like' to 'empty'. Coupled with these conformational changes, the DF subunits rotate 120°. After this rotation, ATP bound at the
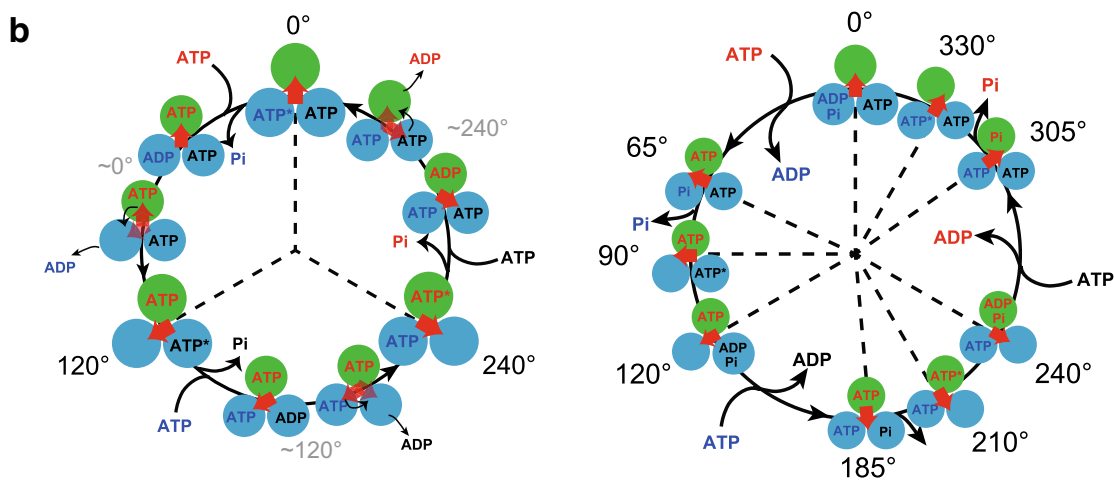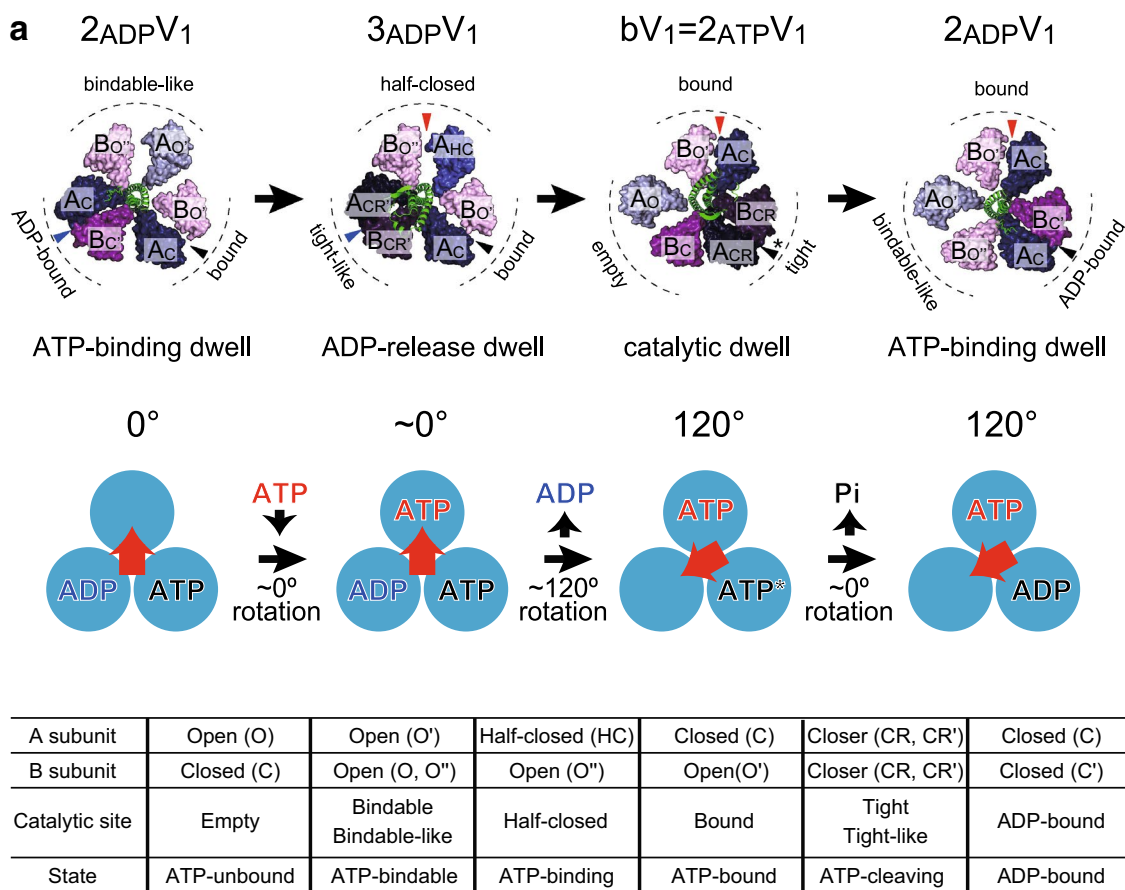
Fig. 10 Chemomechanical coupling scheme of V$_1$-ATPase. **a** Proposed rotation model of *E. hirae* V$_1$-ATPase for 120° rotation [45]. The structure models are based on the crystal structures of 2$_{ADP}$V$_1$ (ATP-binding dwell), 3$_{ADP}$V$_1$ (ADP-release dwell), and bV$_1$ (catalytic dwell). The catalytic sites that bind to nucleotides are indicated by arrowheads (top). Each blue circle represents the chemical state of each catalytic site, and the central red arrow represents the orientation of the rotor DF subunits. ATP* represents the pre- or post-hydrolysis state of ATP (middle). Correspondence table for all catalytic sites observed in the crystal structures of the A$_3$B$_3$ and V$_1$-ATPase (bottom). **b** Possible chemomechanical coupling scheme of *E. hirae* V$_1$-ATPase [44–46, 48, 49] (left) and human F$_1$-ATPase [40] (right) for 360° rotation. 0° is set as the ATP-binding angle for the catalytic site at the 12 O'clock position (green). In the model of *E. hirae* V$_1$-ATPase, ATP bound at 0° is cleaved into ADP and Pi at 240°. Among these, phosphate first dissociates at 240°, and then, ADP release occurs at 240°. Other catalytic sites also obey the same reaction scheme offset by 120° and 240°. In the model of human F$_1$-ATPase, ATP bound at 0° is cleaved into ADP and Pi at 210°, ADP dissociates at 240°, and then, phosphate release occurs at 305°

'tight' site in bV_1 ($= 2_{ATP}V_1$) is cleaved into ADP and phosphate. The release of phosphate, which has a lower affinity than ADP, is coupled with a conformational change from a 'tight' site to 'ADP-bound' site and from an 'empty' site to 'bindable-like' site. Consequently, the rotor DF subunits tilt toward the 'ADP-bound' site, without showing obvious rotation. Finally, it returns to the initial rotational state with 120° rotation (Fig. 10a).

Currently, there are no single-molecule studies on V_1-ATPase from *E. hirae* that directly demonstrate the dwell angles for ATP cleavage, ADP release, and phosphate release at a single catalytic site over one revolution. However, considering the results of single-molecule studies and structural studies, the model for 360° rotation cycle is conceivable [48].

If the ATP-binding angle is defined as 0° in the 360° rotation cycle (Fig. 10b, left), ATP is cleaved at 240°. Then, phosphate is released first at 240°, and finally, ADP is released at 240°. In comparison, the proposed chemomechanical coupling scheme of F_1-ATPase is more complicated. In the case of thermophilic *Bacillus* PS3 F_1-ATPase, ATP cleavage, ADP release, and phosphate release occur at 200°, 240°, and 320° [37], respectively, although the timing of phosphate release is controversial. Furthermore, in the case of human F_1-ATPase, ATP cleavage, ADP release, and phosphate release occur at 210°, 240°, and 305°, respectively (Fig. 10b, right) [40]. The coupling scheme of human F_1-ATPase can be considered a variation of that of thermophilic *Bacillus* PS3 F_1-ATPase, in which the ATP cleavage and the phosphate-release dwells are split into different angles. Of course, it is possible that V_1-ATPase also shows the substeps, because the angles waiting for ADP release and phosphate release have not been directly demonstrated by advanced single-molecule experiments, as has been performed in the case of F_1-ATPase [34, 35, 37]. Furthermore, multiscale molecular dynamics simulations predict the formation of rotational intermediate states of this V_1-ATPase that have not yet been resolved [60]. Interestingly, the recent information-based soft clustering method revealed that thermophilic *Bacillus* PS3 F_1-ATPase makes a small rotational movement during the catalytic dwell triggered by the ATP hydrolysis reaction; this had not been previously resolved using the conventional analysis methods [61]. Such advanced single-molecule techniques and analysis methods may reveal the unresolved reaction scheme and movements of V_1-ATPase.

Future prospects

The recent high-resolution structural studies and single-molecule studies reviewed have begun to clarify the rotation mechanism of V_1-ATPase. By comparing the differences and similarities in the rotation mechanism between V_1-ATPase and F_1-ATPase, we can determine the 'unique' and 'common' mechanisms by which these rotary ATPases function and thereby establish the working principle of rotary ATPases. However, to fully understand the rotation mechanism of rotary ATPases, it is necessary to further improve our 'knowledge and understanding' by designing rotary ATPases with improved, modified, or novel functions based on our current 'knowledge and understanding,' and by experimentally verifying designed proteins. Such a synthetic approach has become a trend in biology and nanobiotechnology [62–67], and this approach will be extremely helpful to understand the mechanisms by which rotary ATPases operate.

References

1. Mitchell P (1966) Chemiosmotic coupling in oxidative and photosynthetic phosphorylation. Biol Rev Camb Philos Soc 41:445–502
2. Boyer PD (1997) The ATP synthase—a splendid molecular machine. Annu Rev Biochem 66:717–749
3. Yoshida M, Muneyuki E, Hisabori T (2001) ATP synthase—a marvellous rotary engine of the cell. Nat Rev Mol Cell Biol 2:669–677
4. von Ballmoos C, Wiedenmann A, Dimroth P (2009) Essentials for ATP synthesis by F1F0 ATP synthases. Annu Rev Biochem 78:649–672
5. Forgac M (2007) Vacuolar ATPases: rotary proton pumps in physiology and pathophysiology. Nat Rev Mol Cell Biol 8:917–929
6. Mulkidjanian AY, Makarova KS, Galperin MY, Koonin EV (2007) Inventing the dynamo machine: the evolution of the F-type and V-type ATPases. Nat Rev Microbiol 5:892–899
7. Bowman EJ, Bowman BJ (2005) V-ATPases as drug targets. J Bioenerg Biomembr 37:431–435
8. Nakano M, Imamura H, Toei M, Tamakoshi M, Yoshida M, Yokoyama K (2008) ATP hydrolysis and synthesis of a rotary motor V-ATPase from *Thermus thermophilus*. J Biol Chem 283:20789–20796
9. Yokoyama K, Muneyuki E, Amano T, Mizutani S, Yoshida M, Ishida M, Ohkuma S (1998) V-ATPase of *Thermus thermophilus* is inactivated during ATP hydrolysis but can synthesize ATP. J Biol Chem 273:20504–20510

10. Gruber G, Manimekalai MS, Mayer F, Muller V (2014) ATP synthases from archaea: the beauty of a molecular motor. Biochim Biophys Acta 1837:940–952

11. Cross RL, Muller V (2004) The evolution of A-, F-, and V-type ATP synthases and ATPases: reversals in function and changes in the H+/ATP coupling ratio. FEBS Lett 576:1–4

12. Muench SP, Trinick J, Harrison MA (2011) Structural divergence of the rotary ATPases. Q Rev Biophys 44:311–356

13. Murata T, Igarashi K, Kakinuma Y, Yamato I (2000) Na+ binding of V-type Na+ -ATPase in *Enterococcus hirae*. J Biol Chem 275:13415–13419

14. Murata T, Yamato I, Kakinuma Y, Leslie AG, Walker JE (2005) Structure of the rotor of the V-Type Na+ -ATPase from *Enterococcus hirae*. Science 308:654–659

15. Murata T, Yamato I, Kakinuma Y, Shirouzu M, Walker JE, Yokoyama S, Iwata S (2008) Ion binding and selectivity of the rotor ring of the Na+ -transporting V-ATPase. Proc Natl Acad Sci USA 105:8607–8612

16. Stewart AG, Sobti M, Harvey RP, Stock D (2013) Rotary ATPases: models, machine elements and technical specifications. Bioarchitecture 3:2–12

17. Kühlbrandt W, Davies KM (2016) Rotary ATPases: a new twist to an ancient machine. Trends Biochem Sci 41:106–116

18. Oot RA, Kane PM, Berry EA, Wilkens S (2016) Crystal structure of yeast V1-ATPase in the autoinhibited state. EMBO J 35:1694–1706

19. Abrahams JP, Leslie AG, Lutter R, Walker JE (1994) Structure at 2.8 A resolution of F1-ATPase from bovine heart mitochondria. Nature 370:621–628

20. Menz RI, Walker JE, Leslie AG (2001) Structure of bovine mitochondrial F(1)-ATPase with nucleotide bound to all three catalytic sites: implications for the mechanism of rotary catalysis. Cell 106:331–341

21. Kagawa R, Montgomery MG, Braig K, Leslie AG, Walker JE (2004) The structure of bovine F1-ATPase inhibited by ADP and beryllium fluoride. EMBO J 23:2734–2744

22. Rees DM, Montgomery MG, Leslie AG, Walker JE (2012) Structural evidence of a new catalytic intermediate in the pathway of ATP hydrolysis by F1-ATPase from bovine heart mitochondria. Proc Natl Acad Sci USA 109:11139–11143

23. Gledhill JR, Montgomery MG, Leslie AG, Walker JE (2007) How the regulatory protein, IF(1), inhibits F(1)-ATPase from bovine mitochondria. Proc Natl Acad Sci USA 104:15671–15676

24. Kabaleeswaran V, Puri N, Walker JE, Leslie AG, Mueller DM (2006) Novel features of the rotary catalytic mechanism revealed in the structure of yeast F1 ATPase. EMBO J 25:5433–5442

25. Kabaleeswaran V, Shen H, Symersky J, Walker JE, Leslie AG, Mueller DM (2009) Asymmetric structure of the yeast F1 ATPase in the absence of bound nucleotides. J Biol Chem 284:10546–10551

26. Cingolani G, Duncan TM (2011) Structure of the ATP synthase catalytic complex (F(1)) from *Escherichia coli* in an autoinhibited conformation. Nat Struct Mol Biol 18:701–707

27. Shirakihara Y, Shiratori A, Tanikawa H, Nakasako M, Yoshida M, Suzuki T (2015) Structure of a thermophilic F1-ATPase inhibited by an epsilon-subunit: deeper insight into the epsilon-inhibition mechanism. FEBS J 282:2895–2913

28. Bowler MW, Montgomery MG, Leslie AG, Walker JE (2007) Ground state structure of F1-ATPase from bovine heart mitochondria at 1.9 A resolution. J Biol Chem 282:14238–14242

29. Noji H, Yasuda R, Yoshida M, Kinosita K Jr (1997) Direct observation of the rotation of F1-ATPase. Nature 386:299–302

30. Yasuda R, Noji H, Kinosita K Jr, Yoshida M (1998) F1-ATPase is a highly efficient molecular motor that rotates with discrete 120 degree steps. Cell 93:1117–1124

31. Yasuda R, Noji H, Yoshida M, Kinosita K Jr, Itoh H (2001) Resolution of distinct rotational substeps by submillisecond kinetic analysis of F1-ATPase. Nature 410:898–904

32. Shimabukuro K, Yasuda R, Muneyuki E, Hara KY, Kinosita K Jr, Yoshida M (2003) Catalysis and rotation of F1 motor: cleavage of ATP at the catalytic site occurs in 1 ms before 40 degree substep rotation. Proc Natl Acad Sci USA 100:14731–14736

33. Ariga T, Muneyuki E, Yoshida M (2007) F1-ATPase rotates by an asymmetric, sequential mechanism using all three catalytic subunits. Nat Struct Mol Biol 14:841–846

34. Adachi K, Oiwa K, Nishizaka T, Furuike S, Noji H, Itoh H, Yoshida M, Kinosita K Jr (2007) Coupling of rotation and catalysis in F(1)-ATPase revealed by single-molecule imaging and manipulation. Cell 130:309–321

35. Nishizaka T, Oiwa K, Noji H, Kimura S, Muneyuki E, Yoshida M, Kinosita K Jr (2004) Chemomechanical coupling in F1-ATPase revealed by simultaneous observation of nucleotide kinetics and rotation. Nat Struct Mol Biol 11:142–148

36. Masaike T, Koyama-Horibe F, Oiwa K, Yoshida M, Nishizaka T (2008) Cooperative three-step motions in catalytic subunits of F(1)-ATPase correlate with 80 degrees and 40 degrees substep rotations. Nat Struct Mol Biol 15:1326–1333

37. Watanabe R, Iino R, Noji H (2010) Phosphate release in F1-ATPase catalytic cycle follows ADP release. Nat Chem Biol 6:814–820

38. Martin JL, Ishmukhametov R, Hornung T, Ahmad Z, Frasch WD (2014) Anatomy of F1-ATPase powered rotation. Proc Natl Acad Sci USA 111:3715–3720

39. Bilyard T, Nakanishi-Matsui M, Steel BC, Pilizota T, Nord AL, Hosokawa H, Futai M, Berry RM (2013) High-resolution single-molecule characterization of the enzymatic states in *Escherichia coli* F1-ATPase. Philos Trans R Soc Lond B Biol Sci 368:20120023

40. Suzuki T, Tanaka K, Wakabayashi C, Saita E, Yoshida M (2014) Chemomechanical coupling of human mitochondrial F1-ATPase motor. Nat Chem Biol 10:930–936

41. Maher MJ et al (2009) Crystal structure of A3B3 complex of V-ATPase from *Thermus thermophilus*. EMBO J 28:3771–3779

42. Numoto N, Hasegawa Y, Takeda K, Miki K (2009) Inter-subunit interaction and quaternary rearrangement defined by the central stalk of prokaryotic V1-ATPase. EMBO Rep 10:1228–1234

43. Nagamatsu Y, Takeda K, Kuranaga T, Numoto N, Miki K (2013) Origin of asymmetry at the intersubunit interfaces of V1-ATPase from *Thermus thermophilus*. J Mol Biol 425:2699–2708

44. Arai S et al (2013) Rotation mechanism of *Enterococcus hirae* V1-ATPase based on asymmetric crystal structures. Nature 493:703–707

45. Suzuki K et al (2016) Crystal structures of the ATP-binding and ADP-release dwells of the V1 rotary motor. Nat Commun 7:13235

46. Minagawa Y et al (2013) Basic properties of rotary dynamics of the molecular motor *Enterococcus hirae* V1-ATPase. J Biol Chem 288:32700–32707

47. Ueno H et al (2014) Torque generation of *Enterococcus hirae* V-ATPase. J Biol Chem 289:31212–31223

48. Iino R, Minagawa Y, Ueno H, Hara M, Murata T (2014) Molecular structure and rotary dynamics of *Enterococcus hirae* V(1)-ATPase. IUBMB Life 66:624–630

49. Iino R, Ueno H, Minagawa Y, Suzuki K, Murata T (2015) Rotational mechanism of *Enterococcus hirae* V1-ATPase by crystal-structure and single-molecule analyses. Curr Opin Struct Biol 31:49–56

50. Shirakihara Y et al (1997) The crystal structure of the nucleotide-free alpha 3 beta 3 subcomplex of F1-ATPase

from the thermophilic *Bacillus* PS3 is a symmetric trimer. Structure 5:825–836

51. Uchihashi T, Iino R, Ando T, Noji H (2011) High-speed atomic force microscopy reveals rotary catalysis of rotorless F-ATPase. Science 333:755–758

52. Liu Q, Leng XH, Newman PR, Vasilyeva E, Kane PM, Forgac M (1997) Site-directed mutagenesis of the yeast V-ATPase A subunit. J Biol Chem 272:11750–11756

53. Hayashi S et al (2012) Molecular mechanism of ATP hydrolysis in F1-ATPase revealed by molecular simulations and single-molecule observations. J Am Chem Soc 134:8447–8454

54. Noji H, Hasler K, Junge W, Kinosita K Jr, Yoshida M, Engelbrecht S (1999) Rotation of *Escherichia coli* F(1)-ATPase. Biochem Biophys Res Commun 260:597–599

55. Imamura H, Takeda M, Funamoto S, Shimabukuro K, Yoshida M, Yokoyama K (2005) Rotation scheme of V1-motor is different from that of F1-motor. Proc Natl Acad Sci USA 102:17929–17933

56. McMillan DGG, Watanabe R, Ueno H, Cook GM, Noji H (2016) Biophysical characterization of a thermoalkaliphilic molecular motor with a high stepping torque gives insight into evolutionary ATP synthase adaptation. J Biol Chem 291:23965–23977

57. Hirata T, Iwamoto-Kihara A, Sun-Wada GH, Okajima T, Wada Y, Futai M (2003) Subunit rotation of vacuolar-type proton pumping ATPase: relative rotation of the G and C subunits. J Biol Chem 278:23714–23719

58. Imamura H, Nakano M, Noji H, Muneyuki E, Ohkuma S, Yoshida M, Yokoyama K (2003) Evidence for rotation of V1-ATPase. Proc Natl Acad Sci USA 100:2312–2315

59. Furuike S, Nakano M, Adachi K, Noji H, Kinosita K Jr, Yokoyama K (2011) Resolving stepping rotation in *Thermus thermophilus*

H(+)-ATPase/synthase with an essentially drag-free probe. Nat Commun 2:233

60. Isaka Y, Ekimoto T, Kokabu Y, Yamato I, Murata T, Ikeguchi M (2017) Rotation mechanism of molecular motor V1-ATPase studied by multiscale molecular dynamics simulation. Biophys J 112:911–920

61. Li CB, Ueno H, Watanabe R, Noji H, Komatsuzaki T (2015) ATP hydrolysis assists phosphate release and promotes reaction ordering in F1-ATPase. Nat Commun 6:10223

62. Schwille P, Diez S (2009) Synthetic biology of minimal systems. Crit Rev Biochem Mol Biol 44:223–242

63. Kay ER, Leigh DA, Zerbetto F (2007) Synthetic molecular motors and mechanical machines. Angew Chem Int Ed Engl 46:72–191

64. Chen L, Nakamura M, Schindler TD, Parker D, Bryant Z (2012) Engineering controllable bidirectional molecular motors based on myosin. Nat Nanotechnol 7:252–256

65. Nakamura M, Chen L, Howes SC, Schindler TD, Nogales E, Bryant Z (2014) Remote control of myosin and kinesin motors using light-activated gearshifting. Nat Nanotechnol 9:693–697

66. Furuta A, Amino M, Yoshio M, Oiwa K, Kojima H, Furuta K (2017) Creating biomolecular motors based on dynein and actin-binding proteins. Nat Nanotechnol 12:233–237

67. DelRosso NV, Derr ND (2017) Exploiting molecular motors as nanomachines: the mechanisms of de novo and re-engineered cytoskeletal motors. Curr Opin Biotechnol 46:20–26

68. Ueno H, Nishikawa S, Iino R, Tabata KV, Sakakihara S, Yanagida T, Noji H (2010) Simple dark-field microscopy with nanometer spatial precision and microsecond temporal resolution. Biophys J 98:2014–2023